Research Article | Vol. 26, No. 23 | 12 Nov 2018 | OPTICS EXPRESS 30944
Optics EXPRESS

# Dynamically tunable multi-lobe laser generation via multifocal curved beam

ENBO XING,[1,5] HUI GAO,[2,5] JIAMIN RONG,[3,5] SI YING. KHEW,[1] HUAGANG LIU,[1] CUNZHU TONG,[4] AND MINGHUI HONG[1,*]

[1]*Department of Electrical and Computer Engineering, National University of Singapore, Singapore 117576, Singapore*
[2]*Wuhan National Laboratory for Optoelectronics, Huazhong University of Science and Technology, 1037 Luoyu Road, Wuhan, 430074, China*
[3]*Temasek Laboratories, Nanyang Technological University, Singapore 637553, Singapore*
[4]*State Key Laboratory of Luminescence and Applications, Changchun Institute of Optics, Fine Mechanics and Physics, Chinese Academy of Sciences, Changchun 130033, China*
[5]*These authors contributed equally to this work.*
**elehmh@nus.edu.sg*

**Abstract:** Beams with curved properties, represented by Airy beam, have already shown potential applications in various fields. Here we propose a simple method to achieve a multifocal curved beam (MCB). The scheme is based on the ability of microspheres to control the distribution of the light field. Combined with the caustic effect, the dynamic control of the beam curvature and the foci can be realized. The simulation results confirm the mechanism behind this phenomenon. Furthermore, MCB is applied experimentally into the end-pumped microchip laser. This work has verified the theory of MCB and achieved a dynamically tunable multi-lobe laser, which has a wide application prospect.



## 1. Introduction

Approximately non-diffracting Airy beam is predicted theoretically in 1979 [1], and the first observation of the Airy beam in both one and two dimensional configurations is demonstrated experimentally in 2007 [2]. Since then the Airy beam has attracted widespread attention and has been applied in a variety of fields [3–14]. Another unique characteristic of Airy beam is the parabolic trajectory during propagation. This feature has demonstrated a wide range of prospects in practical applications [15–20], such as particle manipulation, light-sheet microscopy, laser micromachining, guided discharge, and image signal transmission, etc. The above researches suggest that the beams which do not propagate along straight trajectories have special significance in practical applications. Therefore, some studies have recently been conducted on the implementation of novel types of analogous curved beams [21–28].

Currently, the most common method is based on the research of the Airy beam, relying on the spatial light modulators (SLM) to generate curved beams [2,4–8,13–16]. However, SLM is restricted in its applications due to the large size of pixels, and the ability of the SLM to bend the light at a steep angle is severely limited [21]. Another research direction is to develop new methods to manipulate light, including plane nanostructures, high-precision adaptive reflective mirrors, laser-written cubic-phase plate, and Seidel wave aberrations [21–27]. In addition, recent studies have also shown that the asymmetric dielectric particles can achieve the curved light [27,28]. However, these known solutions usually require complicated designs or elaborate processing methods, which severely limits the further development and applications of curved beams.

A transparent dielectric microsphere is an alternative optical component that is worth considering since it has the ability of redistributing the light field at low propagation loss and is inexpensive. Moreover, very large spherical curvature easily produces optical aberrations, which has also been proved to be able to generate 1D or 2D Airy beam [23]. The transparent

#341828 https://doi.org/10.1364/OE.26.030944
Journal © 2018 Received 20 Aug 2018; revised 13 Oct 2018; accepted 15 Oct 2018; published 9 Nov 2018

Optics EXPRESS

dielectric microsphere has a certain achievement in assisted traditional optical microscopy [29–32]. In the imaging process, there exist side lobes in the oscillatory field behind the central lobe [31]. The properties of the central and side lobes can be determined by incident light with a specified microsphere diameter and material. Although this phenomenon leads to lateral resolution distortion and signal-to-noise ratio reduction, from another point of view, there are additional degrees of freedom to redistribute the light field through the microspheres.

In this paper, we propose a novel approach to realize multifocal curved beam (MCB) by the redistributing the light field though a $SiO_2$ microsphere with off-axis incidence. Compared with previous studies on curved beams, the MCB not only has a tunable curvature, but also a multifocal feature that other curved beams do not possess. The foci are on the curved caustic which is composed of central and side lobes, therefore the MCB is well controlled via the adjustment of off-axis magnitude. Finite-difference time-domain (FDTD) is employed to theoretically analyze the formation mechanism and characteristics for MCB. In the experiment, we use MCB as the pumping source of the microchip laser to obtain dynamically tunable output beam profile.

## 2. Theoretical framework

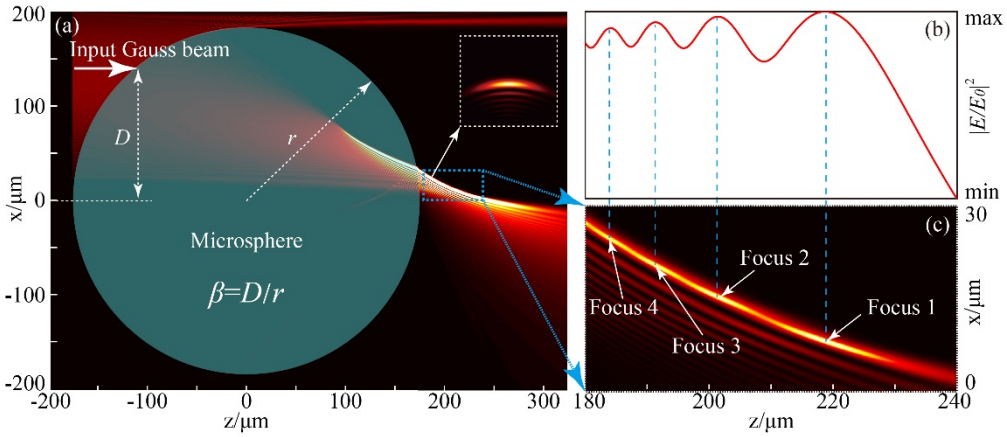


Fig. 1. Principle of the formation of the multifocal curved beam. (a) The generation of curved beams through a dielectric microsphere. The insert is the magnified lateral light field distribution with the z = 183 μm. (b) The relationship between the light field distribution and the z-axis position of the highest intensity curved beam. (c) The magnified image of the curved beam area, and these multiple foci are referred to as Focus 1, 2, 3, 4, respectively.

Figure 1 schematically shows the MCB via a $SiO_2$ microsphere with off-axis incidence. This microsphere has a radius of 175 μm and refractive index of 1.453 at the wavelength of 808 nm. The incident Gaussian light is indicated by the white arrow. The waist radius of 110 μm is smaller than that of the microsphere. A parameter β = D/r is used to define the degree of off-axis illumination between the two axis, where D is off-axis shifting and r is the radius of microsphere. These parameters are indicated in the Fig. 1(a). The field distribution of MCB is calculated by the 2D FDTD solution. As illustrated in Fig. 1(a) with the β value of 0.7, light passes through the upper part of the microsphere and forms a curved envelope of light rays near the surface of microsphere. The reason is that the large spherical aberration of the microsphere causes significant caustics [33]. When the complete caustic surface corresponding to normal on-axis incidence is used as a reference, the off-axis asymmetrically incident light can be considered as only a portion of the caustic surface. The ray envelope therefore exhibits curved features. In Fig. 1(c), Focus 1 to Focus 4 represents four focuses from left to right, respectively. Figure 1(c) shows a magnified image of multi-lobe, the distribution of the light field in the x-z plane is similar to the appearance of propagation

Optics EXPRESS

dynamics of 1D Airy beams [23]. The light field distribution of the trajectory with the highest intensity is discrete, which exhibits the property of multiple foci. The corresponding relative intensities and positions are shown in Fig. 1(b). Additionally, the distribution of light field in x-y plane is calculated by the 3D Zemax software. The white dotted area represents the area size of 30 μm x 30 μm, which indicates that the curved beams formed by the microsphere do not have the characteristic of 2D intensity distribution of the Airy beams.

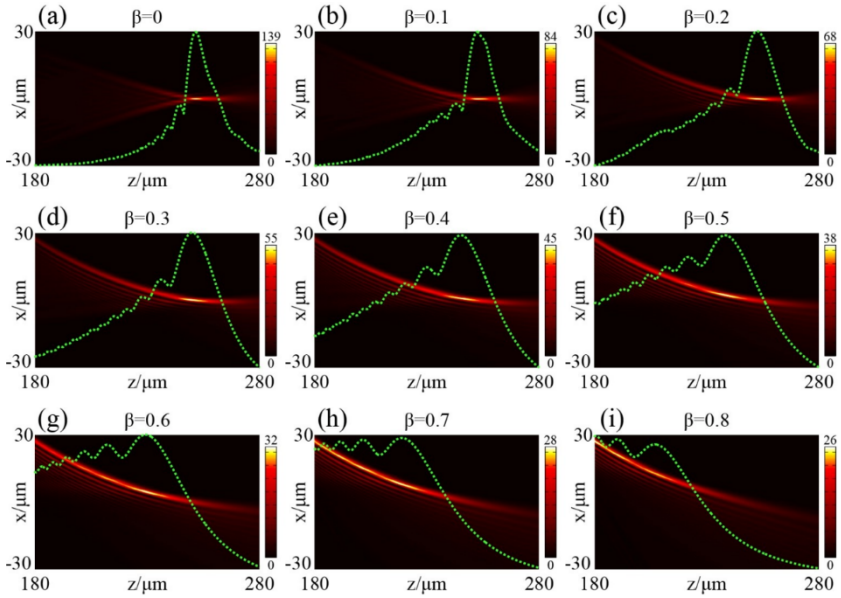


Fig. 2. Relationship between the degree of off-axis incidence (β from 0 to 0.8) and the light field distribution through the microsphere. The green dotted line numerically represents the intensity of the maximum bending beam with respect to the position on z axis.

To further investigate the mechanism behind the MCB, the influence of β value on the light field distribution is simulated by 2D FDTD solution. Figure 2(a) shows a typical intensity contour of light focused by a 175 μm radius microsphere with on-axis incidence. From our previous experiment and simulation results of the microspheres [31], it is known that a series of side lobes appear behind the central lobe due to aberrations. These side lobes are arranged in sequence behind the central lobe and to form a horn-like shape, as shown in Fig. 2(a). When β is greater than 0, the symmetry of the light field distribution is broken, and the overall light field distribution shifts toward the off-axis. The side lobes in the upper part gradually merge with the central lobe to form an arc-shaped high intensity trajectory. The distinct evolution process occurs mainly when β is from 0 to 0.3. With the increase of β, the intensities of the central and the side lobes decrease at different rates. The intensity of the central lobe decreases more rapidly than the side lobe intensity, and consequently the intensities of the side lobes are comparable to that of the central lobe when β exceeds 0.6. The green dotted line numerically represents the intensity of the maximum bending beam with respect to the position on z axis. It can be seen that the intensity of Focus 1 becomes the lowest with β of 0.8. This means that when β is large enough, the intensities of side lobe will be higher than that of the central lobe. and are referred to as Focus 1 to Focus 4 from right to left, which corresponds to Fig. 1(c).

Optics EXPRESS

## 3. Experimental results and discussion

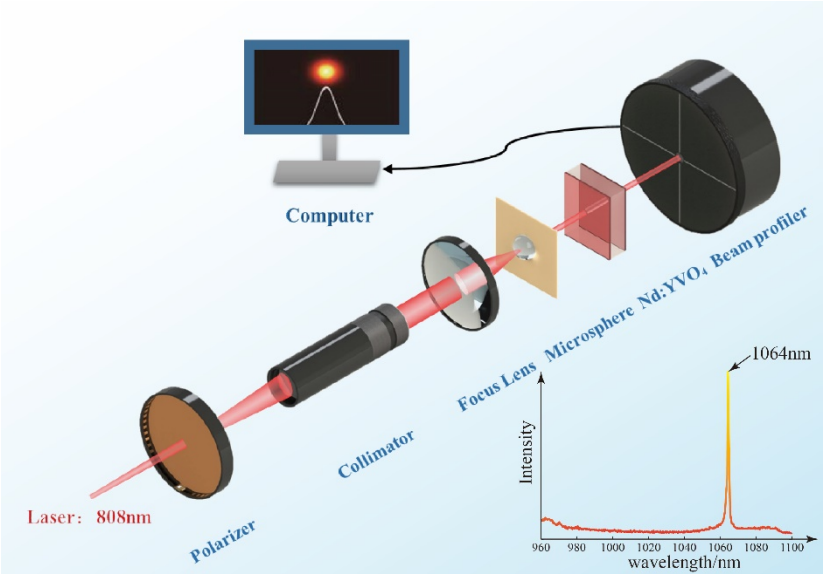


Fig. 3. The experimental setup of the passively Q-switched Nd: YVO4 microchip laser using the MCB as pumping light source and the output spectrum.

Based on the above numerical simulation, it can be found that the spatial separation of these focal points in x direction is only a few micrometers, which is difficult to directly measure experimentally. Therefore, the MCB as a pump light is introduced into an end-pumped microchip laser, in order to experimentally verify the optical properties of the MCB. The transverse multiple lobes can reflect the x-axis pump light, and the difference in the output intensity of each lobe indicates that the position in the z direction is different. Figure 3 shows the experimental configuration for MCB-assisted pumping microchip laser and the output spectrum with the wavelength of 1064 nm. The gain medium is a-axis cut Nd: $YVO_4$ crystal doped with 3.0 at. % $Nd^{3+}$ ions and dimensions of 3 mm x 3 mm x 0.6 mm. The pump surface is coated for high reflectivity (HR, R > 99.8%) at 1064 nm and high transmissivity (HT, T > 96%) at 808 nm, which is used as the input mirror, the opposite surface is coated for HT (T > 96%) at 1064 nm. The pumping source is focused to the diameter of 220 μm through a collimating and a focusing elements, and then it is directly incident on a $SiO_2$ microsphere with the radius of 175 μm. For the convenient adjustment of the microsphere position, we have drilled several small holes in a 150 μm metal sheet by using a nanosecond pulse fiber laser for mounting the microsphere. β is controlled with 1-micron class accuracy by adjusting the position of microsphere. The beam characteristics and output power are measured by a beam profiler.

Optics EXPRESS

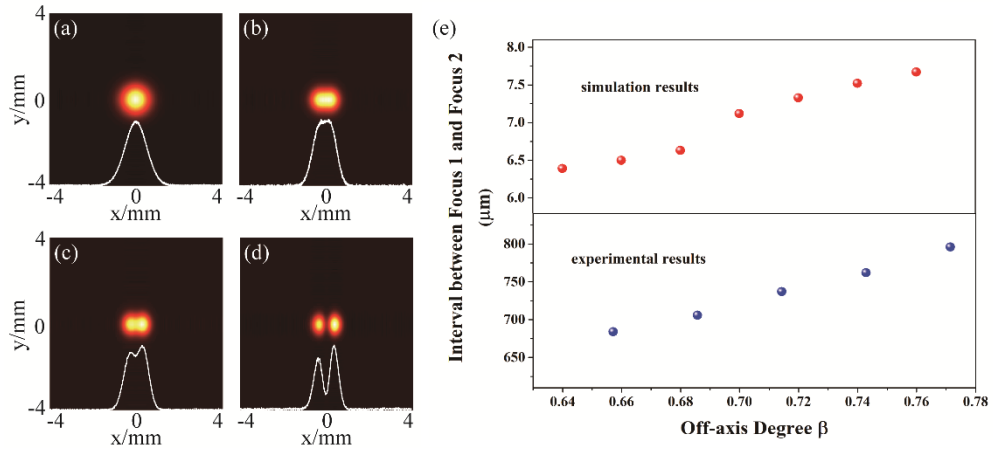


Fig. 4. (a) to (d) show the evolution of the experimentally output beam profilers as the increase of β. (e) shows the effect of β on the intervals between Focus 1 and Focus 2 for the simulation and experiment.

The characteristics of the output beams could be transferred from the pump beams (MCB). Therefore, from the output beams of the laser, we can infer the properties of the pump beams, especially the shape of beams. Taking advantage of the divergence angle of the microchip laser, output beams can be measured at a far distance, and the magnified images make analyze easier. In the initial experiment, the optical axis of the pumping light passes through the center of the microsphere and is perpendicularly incident on the laser crystal. At this time, the pumping light forms a circular focused spot inside the crystal, and one circular output beam is indicated in Fig. 4(a). Subsequently, to study the effect of β value on the output performance of microchip laser, the β is adjusted by controlling the position of microsphere horizontally. The value of input power is selected as a constant of 120.3 mW. As β increases, the circular beam profile (β = 0) becomes an elliptical beam profile (β = 0.49), a peanut-shaped beam profile (β = 0.6), and then splits into two lobe profiles (β = 0.66) sequentially, corresponding to Figs. 4(a) to 4(d), respectively. Theoretically, we have calculated the interval between the Focus 1 and Focus 2 along the x direction are plotted in red symbols in Fig. 4(e). There is a positive correlation between the separation amplitude and β, which is in good agreement with the experimental results. It should be noted that although the output beam can be controlled by adjusting the value of β, an excessively high β causes the power density of the pumping light to decrease, resulting in a high lasing threshold.

Optics EXPRESS

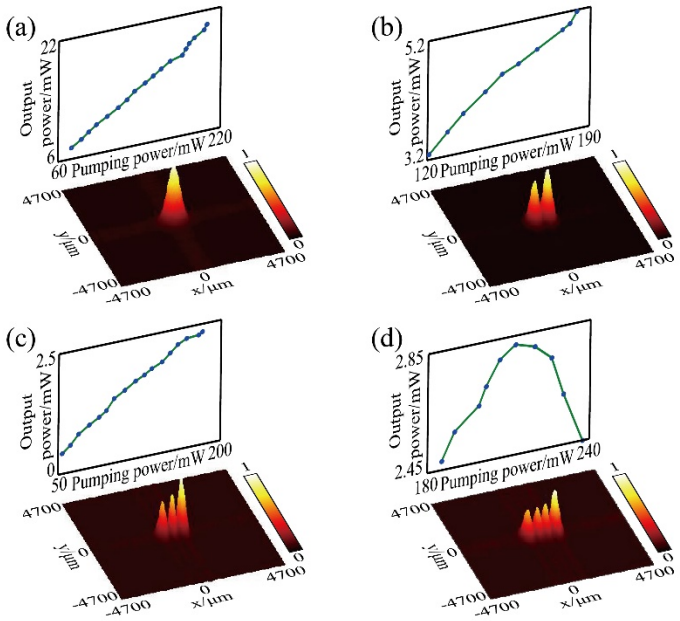


Fig. 5. Dynamically tunable laser output performance using the MCB as the pumping source. (a) to (d) represents the 3D output beam profile and output power curves, when β is 0, 0.71, 0.82, and 0.82, respectively. The output beams from (a) to (c) are pumped by the power of 120.3 mW, and (d) is the power of 201.5 mW.

Finally, we further demonstrate the output performance of end-pumped microchip laser using MCB as the pumping source. The most outstanding advantage of using MCB is that the intensity profile of output beam can be regulated dynamically by adjusting the position of the microsphere. Figures 5(a) to 5(d) shows 3D beam intensity profiles and corresponding power curves from single lobe to four lobes output, when β is 0, 0.71, 0.82, respectively. Figures 5(a) to 5(c) are obtained from the input power of 120.3 mW. The four lobes output profile courses at the higher input power of 201.5 mW and shown in Fig. 5(d), due to the threshold of the fourth lobe being higher than that of the other lobes. At the same time, thermal rollover of output power occurs, which is attributed mainly to the thermal lens effect, the birefringence and distortion in the gain medium caused by heat accumulation. Therefore, the laser operates in an unstable zone with the high injection power. Next, we mainly analyze the characteristics of these different output lobes. On one hand, multiple output lobes originate from the same laser output beam, which is evidenced by the expansions of both area and location of the lobes as the distance for measuring intensity profile increases. This feature is consistent with the phenomenon of a single output beam with divergence angle. On the other hand, although the intensity distribution is similar to the cross-sectional intensity distribution of high-order transverse modes, this is based on the MCB pumping from the perspective of the generation mechanism, rather than from the support of higher-order modes in resonant cavity. The above theoretical analysis provides a convenient method for dynamically tunable laser output performance. Furthermore, the lasers with multi-lobe output have a wide range of applications in high-speed laser scanning [34,35], multi beams microfabrication [36], advanced laser velocimetry [37], and multifocal optical data recording [38].

## 4. Conclusions

In summary, multifocal curved beams are achieved by redistributing the light field using a transparent microsphere. By adjusting the relative position between an off-axis Gaussian beam and a microsphere, we effectively control the curvature of the beam and foci. The

Optics EXPRESS

simulation results show that there are obvious points of intensity concentration on the trajectory of the curved beams, and these focal points are derived from the central and side lobes. Therefore, these well-manipulated characteristics are also of positive significance to theoretical design and experimental operation. Additionally, the MCB can be used as the pump source of the microchip laser experimentally, and obtain dynamically tunable multi-lobe output characteristics, which has many potential applications.

## Funding

Open Project of the State Key Laboratory of Luminescence and Applications (SKLA-2018-09); National Research Foundation, Prime Minister's Office, Singapore under its Competitive Research Programme (CRP Award No. NRF-CRP15-2015-04)

## References

1. M. V. Breey and N. L. Balazs, "Nonspreading wave packets," Am. J. Phys. **47**(3), 264–267 (1979).
2. G. A. Siviloglou, J. Broky, A. Dogariu, and D. N. Christodoulides, "Observation of accelerating Airy beams," Phys. Rev. Lett. **99**(21), 213901 (2007).
3. P. Zhang, Y. Hu, T. Li, D. Cannan, X. Yin, R. Morandotti, Z. Chen, and X. Zhang, "Nonparaxial Mathieu and Weber Accelerating Beams," Phys. Rev. Lett. **109**(19), 193901 (2012).
4. Y. Hu, D. Bongiovanni, Z. Chen, and R. Morandotti, "Multipath multicomponent self-accelerating beams through spectrum-engineered position mapping," Phys. Rev. A. **88**(4), 043809 (2013).
5. K. Dholakia and T. Čižmár, "Shaping the future of manipulation," Nat. Photonics **5**(6), 335–342 (2011).
6. J. Baumgartl, M. Mazilu, and K. Dholakia, "Optically mediated particle clearing using Airy wavepackets," Nat. Photonics **2**(11), 675–678 (2008).
7. J. Broky, G. A. Siviloglou, A. Dogariu, and D. N. Christodoulides, "Self-healing properties of optical Airy beams," Opt. Express **16**(17), 12880–12891 (2008).
8. G. A. Siviloglou, J. Broky, A. Dogariu, and D. N. Christodoulides, "Ballistic dynamics of Airy beams," Opt. Lett. **33**(3), 207–209 (2008).
9. A. Chong, W. H. Renninger, D. N. Christodoulides, and F. W. Wise, "Airy–Bessel wave packets as versatile linear light bullets," Nat. Photonics **4**(2), 103–106 (2010).
10. L. Li, T. Li, S. M. Wang, C. Zhang, and S. N. Zhu, "Plasmonic Airy beam generated by in-plane diffraction," Phys. Rev. Lett. **107**(12), 126804 (2011).
11. P. Polynkin, M. Kolesik, and J. Moloney, "Filamentation of femtosecond laser Airy beams in water," Phys. Rev. Lett. **103**(12), 123902 (2009).
12. P. Polynkin, M. Kolesik, J. V. Moloney, G. A. Siviloglou, and D. N. Christodoulides, "Curved plasma channel generation using ultraintense Airy beams," Science **324**(5924), 229–232 (2009).
13. S. Jia, J. C. Vaughan, and X. Zhuang, "Isotropic three-dimensional super-resolution imaging with a self-bending point spread function," Nat. Photonics **8**(4), 302–306 (2014).
14. J. Zhao, I. D. Chremmos, D. Song, D. N. Christodoulides, N. K. Efremidis, and Z. Chen, "Curved singular beams for three-dimensional particle manipulation," Sci. Rep. **5**(1), 12086 (2015).
15. T. Vettenburg, H. I. C. Dalgarno, J. Nylk, C. Coll-Lladó, D. E. K. Ferrier, T. Čižmár, F. J. Gunn-Moore, and K. Dholakia, "Light-sheet microscopy using an Airy beam," Nat. Methods **11**(5), 541–544 (2014).
16. J. Nylk, K. McCluskey, M. A. Preciado, M. Mazilu, Z. Yang, F. J. Gunn-Moore, S. Aggarwal, J. A. Tello, D. E. K. Ferrier, and K. Dholakia, "Light-sheet microscopy with attenuation-compensated propagation-invariant beams," Science Advanced **4**, 4817 (2018).
17. M. Clerici, Y. Hu, P. Lassonde, C. Milián, A. Couairon, D. N. Christodoulides, Z. Chen, L. Razzari, F. Vidal, F. Légaré, D. Faccio, and R. Morandotti, "Laser-assisted guiding of electric discharges around objects," Science Advanced **1**(5), e1400111 (2015).
18. Y. Liang, Y. Hu, D. Song, C. Lou, X. Zhang, Z. Chen, and J. Xu, "Image signal transmission with Airy beams," Opt. Lett. **40**(23), 5686–5689 (2015).
19. A. Mathis, F. Courvoisiera, L. Froehly, L. Furfaro, M. Jacquot, P. A. Lacourt, and J. M. Dudley, "Micromachining along a curve: Femtosecond laser micromachining of curved profiles in diamond and silicon using accelerating beams," Appl. Phys. Lett. **101**(7), 071110 (2012).
20. E. Greenfield, M. Segev, W. Walasik, and O. Raz, "Accelerating Light Beams along Arbitrary Convex Trajectories," Phys. Rev. Lett. **106**(21), 213902 (2011).
21. M. Henstridge, C. Pfeiffer, D. Wang, A. Boltasseva, V. M. Shalaev, A. Grbic, and R. Merlin, "Accelerating light with metasurfaces," Optica **5**(6), 678–681 (2018).
22. I. Epstein and A. Arie, "Arbitrary Bending Plasmonic Light Waves," Phys. Rev. Lett. **112**(2), 023903 (2014).
23. D. G. Papazoglou, S. Suntsov, D. Abdollahpour, and S. Tzortzakis, "Tunable intense Airy beams and tailored femtosecond laser filaments," Phys. Rev. A **81**(6), 061807 (2010).
24. D. Abdollahpour, S. Suntsov, D. G. Papazoglou, and S. Tzortzakis, "Spatiotemporal Airy Light Bullets in the Linear and Nonlinear Regimes," Phys. Rev. Lett. **105**(25), 253901 (2010).

Optics EXPRESS


25. Z. Cai, Y. Liu, C. Zhang, J. Xu, S. Ji, J. Ni, J. Li, Y. Hu, D. Wu, and J. Chu, "Continuous cubic phase microplates for generating high-quality Airy beams with strong deflection," Opt. Lett. **42**(13), 2483–2486 (2017).
26. J. Ma, Y. Li, Q. Yu, Z. Yang, Y. Hu, and J. Chu, "Generation of high-quality tunable Airy beams with an adaptive deformable mirror," Opt. Lett. **43**(15), 3634–3637 (2018).
27. L. Yue, O. V. Minin, Z. Wang, J. N. Monks, A. S. Shalin, and I. V. Minin, "Photonic hook: a new curved light beam," Opt. Lett. **43**(4), 771–774 (2018).
28. A. S. Ang, A. Karabchevsky, I. V. Minin, O. V. Minin, S. V. Sukhov, and A. S. Shalin, "'Photonic Hook' based optomechanical nanoparticle manipulator," Sci. Rep. **8**(1), 2029 (2018).
29. L. Li, W. Guo, Y. Yan, S. Lee, and T. Wang, "Label-free super-resolution imaging of adenoviruses by submerged microsphere optical nanoscopy," Light Sci. Appl. **2**, e104 (2013).
30. Z. Wang, W. Guo, L. Li, B. Luk'yanchuk, A. Khan, Z. Liu, Z. Chen, and M. Hong, "Optical virtual imaging at 50 nm lateral resolution with a white-light nanoscope," Nat. Commun. **2**(1), 218 (2011).
31. Y. Yan, L. Li, C. Feng, W. Guo, S. Lee, and M. Hong, "Microsphere-coupled scanning laser confocal nanoscope for sub-diffraction-limited imaging at 25 nm lateral resolution in the visible spectrum," ACS Nano **8**(2), 1809–1816 (2014).
32. L. Chen, Y. Zhou, M. Wu, and M. Hong, "Remote-mode microsphere nano-imaging: new boundaries for optical microscopes," Opto-Electronic Advances **1**(1), 170001 (2018).
33. M. Avendaño-Alejo, L. Castañeda, and I. Moreno, "Properties of caustics produced by a positive lens: meridional rays," J. Opt. Soc. Am. A **27**(10), 2252–2260 (2010).
34. E. Xing, J. Rong, S. Y. Khew, C. Tong, and M. Hong, "Thermal lens effect for optimizing a passively Q-switched 1064nm laser," Appl. Phys. Express **11**(6), 062702 (2018).
35. L. Wang, C. Tong, Y. Zeng, Y. Yang, H. Peng, S. Tian, H. Wu, and L. Wang, "Bragg reflection waveguide twin-beam lasers," Laser Phys. **23**(10), 105802 (2013).
36. S. Maruo and J. T. Fourkas, "Recent progress in multiphoton microfabrication," Laser Photonics Rev. **2**(1–2), 100–111 (2008).
37. B. Wang, Q. Liao, H. A. Bootsma, and P.-F. Wang, "A dual-beam dual-camera method for a battery-powered underwater miniature PIV (UWMPIV) system," Exp. Fluids **52**(6), 1401–1414 (2012).
38. X. Li, Y. Cao, N. Tian, L. Fu, and M. Gu, "Multifocal optical nanoscopy for big data recording at 30 TB capacity and gigabits/second data rate," Optica **2**(6), 567–570 (2015).